International Journal of Nanomedicine

Dovepress

open access to scientific and medical research

Open Access Full Text Article

ORIGINAL RESEARCH

Nanozyme Decorated Metal-Organic Framework Nanosheet for Enhanced Photodynamic Therapy Against Hypoxic Tumor

Jiong Li[1], Dongqin Lei[1], Yanbing Cao[2,3], Fuli Xin[2,3], Zhenxi Zhang[1], Xiaolong Liu[2,3], Ming Wu[2,3], Cuiping Yao[1]

[1]Key Laboratory of Biomedical Information Engineering of Ministry of Education, Institute of Biomedical Photonics and Sensing, School of Life Science and Technology, Xi'an Jiaotong University, Xi'an, 710049, People's Republic of China; [2]The United Innovation of Mengchao Hepatobiliary Technology Key Laboratory of Fujian Province, Mengchao Hepatobiliary Hospital of Fujian Medical University, Fuzhou, 350025, People's Republic of China; [3]Mengchao Med-X Center, Fuzhou University, Fuzhou, 350116, People's Republic of China

Correspondence: Ming Wu, Mengchao Hepatobiliary Hospital of Fujian Medical University, 312 Xi Hong Road, Fuzhou, 350025, People's Republic of China, Email wmmj0419@163.com; Cuiping Yao, School of Life Science and Technology, Xi'an Jiaotong University, 28 Xian Ning West Road, Xi'an, 710049, People's Republic of China, Email zsycp@xjtu.edu.cn

Introduction: Photodynamic therapy (PDT) has attracted increasing attention in the clinical treatment of epidermal and luminal tumors. However, the PDT efficacy in practice is severely impeded by tumor hypoxia and the adverse factors associated with hydrophobic photosensitizers (PSs), including low delivery capacity, poor photoactivity and limited ROS diffusion. In this study, Pt nanozymes decorated two-dimensional (2D) porphyrin metal-organic framework (MOF) nanosheets (PMOF@HA) were fabricated and investigated to conquer the obstacles of PDT against hypoxic tumors.

Materials and Methods: PMOF@HA was synthesized by the coordination of transition metal iron (Zr^{4+}) and PS (TCPP), in situ generation of Pt nanozyme and surface modification with hyaluronic acid (HA). The abilities of hypoxic relief and ROS generation were evaluated by detecting the changes of O_2 and $^1O_2$ concentration. The cellular uptake was investigated using flow cytometry and confocal laser scanning microscopy. The SMMC-7721 cells and the subcutaneous tumor-bearing mice were used to demonstrate the PDT efficacy of PMOF@HA in vitro and in vivo, respectively.

Results: Benefiting from the 2D structure and inherent properties of MOF materials, the prepared PMOF@HA could not only serve as nano-PS with high PS loading but also ensure the rational distance between PS molecules to avoid aggregation-induced quenching, enhance the photosensitive activity and promote the rapid diffusion of generated radical oxide species (ROS). Meanwhile, Pt nanozymes with catalase-like activity effectively catalyzed intratumoral overproduced H_2O_2 into O_2 to alleviate tumor hypoxia. Additionally, PMOF@HA, with the help of externally coated HA, significantly improved the stability and increased the cell uptake by CD44 overexpressed tumor cells to strengthen O_2 self-supply and PDT efficacy.

Conclusion: This study provided a new strategy of integrating 2D porphyrin MOF nanosheets with nanozymes to conquer the obstacles of PDT against hypoxic tumors.

Keywords: 2D porphyrin MOF, hypoxic relief, Pt nanozyme, photodynamic therapy

Introduction

Photosensitizer (PS), as one of the key elements, plays a significant role in tumor PDT.[1] Among them, porphyrin and its derivatives are an important class of PSs, and the major components of commercial Photofrin®, Ameluz® and Levulan® approved by FDA are porphyrins or their precursors.[2] However, porphyrins with robust hydrophobicity, easy aggregation and poor targeting ability severely compromise the clinical efficacy of PDT against tumors.[3–5]

2D nanomaterial with thin planar structure provides an excellent platform to enhance dispersity and facilitate effective delivery of PSs,[6] and different categories of 2D nanomaterials (eg graphene oxide and its derivatives, black phosphorus, metal oxides, etc) have been reported to carry PSs by adsorbing them on the surface of nanosheets or as nano-PSs directly for in vivo

Received: 29 February 2024
Accepted: 3 September 2024
Published: 19 September 2024

PDT.[7–11] Unfortunately, these approaches still suffer from varying degrees of aggregation-induced quenching and confined ROS diffusion of PSs, thereby diminishing their photoactivity and subsequent ROS generation.[12,13] Recently, 2D metal-organic frameworks (MOFs) incorporating porphyrins as organic ligands have attracted increasing attention in PDT,[14–16] which could not only be used as nano-PSs to enhance PS loading capacity but also avoid self-quenching issues and facilitate the rapid diffusion of generated ROS, ascribing to the excellent frame structure and high porosity.[17,18] Additionally, 2D structure offers extra numerous benefits such as heightened responsiveness to external laser stimulation due to the thin nature of the nanostructure for more exposed active sites, a substantial surface area conducive to co-delivery of other functional components,[19] and the easily modifiable surface for enhanced internalization of tumor cells by ornamenting target ligands like hyaluronic acid (HA), folic acid (FA) or other moieties.[20–22]

However, hypoxic microenvironment caused by rapid cancer cells proliferation and abnormal tumor blood vessels can significantly undermine the effectiveness of O_2-dependent PDT.[23] To relieve tumor hypoxia, many efforts have been made to boost intratumoral O_2 level. Some studies have adopted O_2-replenishing system (eg hemoglobin[24] and perfluorocarbon[25,26]) to deliver O_2 directly to tumor site. However, their abilities of hypoxic relief are restricted due to the O_2-carrying materials always suffering from limited O_2 loading capacity and premature O_2 leakage in circulation. Considering the overproduction of H_2O_2 at tumor site, O_2-evolving enzymatic materials were used to decompose H_2O_2 into O_2. This strategy can not only continuously supply O_2 for tumor reoxygenation-based therapy but also lower the H_2O_2 concentration inside the tumor that is closely related to tumor invasiveness and metastasis.[23] Catalase with excellent biosafety and biocompatibility has been reported to catalyze H_2O_2 decomposition for tumor hypoxic relief, but the bio-enzymes with fragile nature are much easier to degrade and deactivate during the process of material fabrication and in vivo delivery.[27,28] On the contrary, as an artificial nanomaterial with enzyme-like activity, nanozyme with facile synthesis and stable property has been extensively explored in various biochemical reactions, and catalase-like nanozyme can be used as an alternative to catalase for H_2O_2 decomposition and O_2 production in tumor.[29,30] Among them, Pt nanoparticles exhibit superior stability compared to other common catalysts such as MnO_2 and do not undergo self-consumption during the catalytic reaction of H_2O_2 decomposition.[31] Therefore, Pt nanoparticle was usually considered to be an ideal nanozyme to decompose H_2O_2 into O_2. There were amounts of studies about Pt nanozymes loaded porphyrin MOFs to enhance PDT by regulating tumor hypoxic microenvironment.[32–36] However, most of those MOFs were with 3D structure. In comparison, 2D MOF nano-PSs with huge advantages, including the larger specific surface to in situ generate Pt nanoparticles, more exposed catalytic sites and easier to contact and react with H_2O_2 when Pt nanoparticles decorated on the lamellar structure, were deserved to deeply develop.

Herein, we constructed Pt nanozymes decorated 2D porphyrin MOF nanosheets with further surface modification of HA (abbreviated as PMOF@HA) to enhance PDT efficacy against hypoxic tumors (Scheme 1). Specifically, the 2D porphyrin MOF nanosheets were fabricated by coordination of TCPP, a porphyrin PS, and the transition metal iron (Zr^{4+}), which not only could serve as nano-PSs to improve delivery efficiency, strengthen photoactivity and promote ROS diffusion, but also provide a broad loading platform for in situ decoration of Pt nanozymes. The O_2 produced significantly alleviated the tumor hypoxic microenvironment, then rapidly transforming to cytotoxic $^1O_2$ induced by the photocatalytic activity of 2D MOF nanosheet under 670 nm laser irradiation. Furthermore, the outer layer of HA, coated through electrostatic interaction, could further enhance the aforementioned functions of PMOF@HA by promoting the targeted uptake of CD44-overexpressing tumor cell. Consequently, the Pt nanozymes decorated and HA coated PMOF@HA nanosheets could achieve CD44 targeting and in situ self-supply of O_2 to intensify PDT efficacy against hypoxic tumors.

Materials and Methods

Materials and Instruments

Zirconium chloride ($ZrCl_4$), tetrakis (4-carboxyphenyl) porphyrin (TCPP), chloroplatinic acid hexahydrate ($H_2PtCl_6{\cdot}6H_2O$), hyaluronic acid (HA, Mw = 75000 Da), Tris (4, 7-diphenyl-1, 10-phenanthroline) ruthenium (II) dichloride complex ($[Ru(dpp)_3]Cl_2$) were purchased from Aladdin (Shanghai, PRC). 2, 7-dichlorodihydrofluorescein diacetate (DCFH-DA) was purchased from J&K Scientific. The human hepatocellular carcinoma-line SMMC-7721 cells (ATCC, Manassas, VA) and human renal epithelial cells 293T (ATCC, Manassas, VA) were cultured in DMEM medium

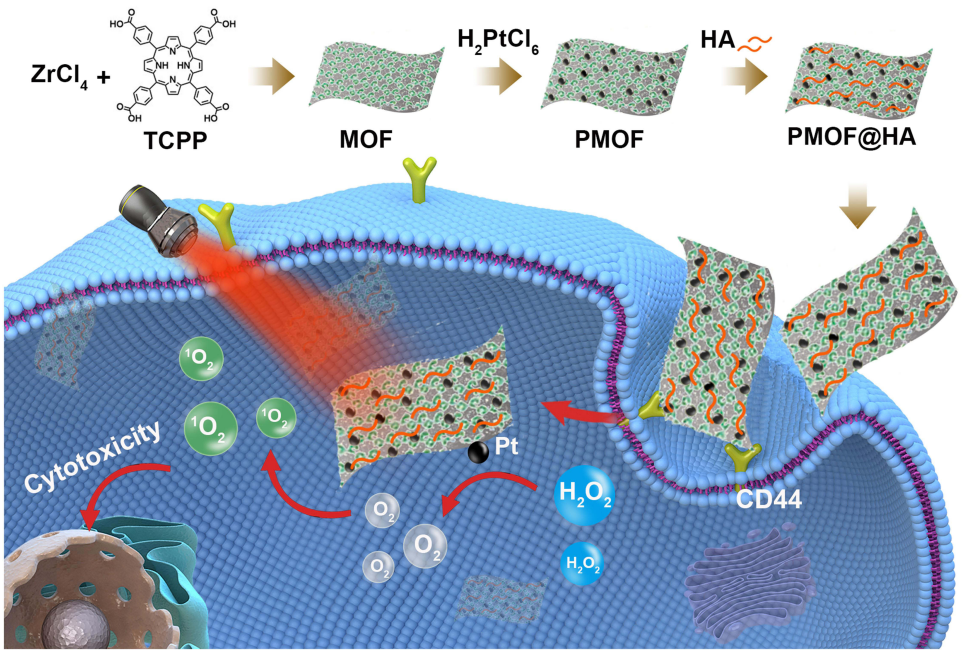

Scheme 1 Schematic illustration of the preparation, hypoxic regulation and photodynamic therapy of PMOF@HA nanosheets.

containing 10% fetal bovine serum (FBS) in the standard condition. Deionized water (ddH_2O, 18.2 MΩ cm) was supplied by a Milli-Q Gradient System (Millipore Corporation, Bedford, MA, USA). If not specified, all other chemicals were used as received.

The morphologies of MOF nanosheets were evaluated using transmission electron microscopy (TEM, FEI Company). The thickness of nanosheets were detected by an atomic force microscopy (AFM). Zeta potentials were measured using a Zetasizer Nano-ZS system (Malvern Instruments, MA). The 670 nm laser (Diode Laser System, BWT Beijing Ltd) was used to exert photodynamic therapy. The cell uptake was analyzed by a confocal laser scanning microscope (CLSM, Zeiss LSM780) and a flow cytometry (BD FACSVerse^{TM}). Live and death assay and ROS generation assay were observed by a fluorescence microscopy (Zeiss Axio Vert.A1, Germany).

Synthesis of PMOF@HA Nanosheets

Synthesis of MOF Nanosheets

4 mg of $ZrCl_4$, 4 mg of TCPP and 100 μL of formic acid were all dissolved in 2 mL DMF. After oscillation, 48 μL of ddH_2O was added into the mixture to promote nucleation. The mixture was heated to 120 °C for 24 h, and then allowed to cool to room temperature naturally. The crude products were washed with anhydrous ethanol and collected by centrifugation at 10,000 rpm. Finally, the MOF nanosheets were re-dispersed in 2 mL anhydrous ethanol for further usage.

Synthesis of Platinum Nanoparticles Decorated MOF Nanosheets (PMOF)

Firstly, 1 mL of the aforementioned MOF nanosheets solution was centrifugated at 10,000 rpm, and the precipitate was re-dispersed in 2 mL of ddH_2O. Then, 5 μL of $H_2PtCl_6 \cdot 6H_2O$ (100 mg/mL) were added into the above solution. After thorough oscillation, the mixture was mixed with $NaBH_4$ solution and allowed to react for 2 min. Finally, the PMOF nanosheets were washed using ddH_2O and obtained by centrifugation at 13,000 rpm.

Synthesis of HA-Coated PMOF

50 μL of HA solution (10 mg/mL) were added into the PMOF nanosheets solution. After sonication, the mixture was left to oscillate at 4 °C overnight. Then, the PMOF@HA nanosheets were collected by centrifugation at 13,000 rpm to remove any unmodified HA. Using the same procedure described, MOF@HA nanosheets without Pt nanoparticles could be obtained by directly coating HA on the surface of MOF nanosheets.

O_2 and Singlet Oxygen ($^1O_2$) Generation Detection

A portable dissolved oxygen detector (INESA, JPBJ-608) was used to evaluate the O_2 level in the solution. In brief, PMOF@HA nanosheets (TCPP: 20 μg) were added into 5 mL ddH_2O containing 2 mM of H_2O_2. The dissolved oxygen probe was immediately immersed in the above mixture, and the O_2 concentration in the solution was measured at different time points.

$^1O_2$ production was monitored by the singlet oxygen sensor green (SOSG) agent. 1 mL PMOF@HA solution (TCPP: 20 μg) containing SOSG probe (5 mM) was irradiated under 670 nm laser (50 mW/cm^2), and the corresponding fluorescence spectra were recorded (Ex: 480 nm).

To assess the enhancement of $^1O_2$ production facilitated by the O_2 self-supply ability of PMOF@HA nanosheets, 1 mL of PMOF@HA solution (TCPP: 20 μg) containing SOSG probe (5 mM) and H_2O_2 (2 mM) was mixed for 10 min. Then, the mixture was subjected to irradiation under 670 nm laser. Finally, the fluorescence spectra of the mixture were recorded timely (Ex: 480 nm).

Cellular Uptake

Firstly, we evaluate the CD44 expression in SMMC-7721 and 293T cells respectively using a flow cytometer. Next, PMOF nanosheets were dispersed in ddH_2O containing 10 μM of Cy5 dye. After oscillation for 4 h, the above mixture was centrifugated to remove the unloaded Cy5 and collect the precipitates (Cy5 labelled PMOF). This material was further modified with HA to obtain Cy5 labelled PMOF@HA. Then, the cells were treated with fresh medium containing Cy5 labelled PMOF@HA nanosheets (TCPP: 40 μg/mL). After culture for 4 h or 8 h, the cells were analyzed by flow cytometry. To further visually assess the impact of HA modification on the cellular uptake of PMOF@HA nanosheets, SMMC-7721 cells pre-treated with or without HA were co-incubated with Cy5 labelled PMOF@HA nanosheets (TCPP: 40 μg/mL) for 8 h. Finally, the cells were stained with DAPI, and observed under CLSM.

Intracellular O_2 and ROS Level Detection

SMMC-7721 cells were cultured for 24 h under normoxic (20% oxygen) or hypoxic (2% oxygen) conditions. Then, PMOF@HA or MOF@HA (TCPP: 80 μg/mL) was added into the cell medium. After culture for another 8 h, the cells were exposed to fresh medium containing 2 μM $[Ru(dpp)_3]Cl_2$ for another 30 min. Finally, the cells were observed using a fluorescence microscopy.

For the assessment of intracellular ROS level, SMMC-7721 cells were cultured for 24 h under normoxic (20% oxygen) or hypoxic (2% oxygen) conditions. Then, PMOF@HA or MOF@HA (TCPP: 80 μg/mL) was added into the cell medium. After culture for another 8 h, fresh medium containing 40 μM of DCFH-DA probe was added into the cells for 15 min incubation. Subsequently, the cells washed with PBS buffer and exposed under a 670 nm laser (50 mW/cm^2) for 5 min. Immediately, the cells were observed using a fluorescence microscopy.

Anti-Tumor Effect in vitro

Firstly, SMMC-7721 cells were incubated with PMOF@HA nanosheets at different concentrations (TCPP: 0, 15, 30, 60, 120, 180 and 240 μg/mL) for 48 h. Afterward, the cell viabilities were detected using CCK-8 assay kit according to the manufacturer's instruction.

To evaluate the effectiveness of PDT in killing cancer cells via PMOF@HA nanosheets, SMMC-7721 cells cultured for 24 h under normoxic (20% oxygen) or hypoxic (2% oxygen) conditions. Then, different concentrations (TCPP: 0, 15, 30, 60 and 120 μg/mL) of PMOF@HA or MOF@HA nanosheets were added into the cell medium. After co-culturing for another 8 h, the cells were exposed under a 670 nm laser (50 mW/cm^2) for 5 min. Finally, the cell viabilities were assessed using CCK-8 assay kit, stained with calcein AM and PI for live/death staining assay, or stained with Annexin V-FITC and PI for apoptosis assay.

Hemolysis Assay

The red blood cells were collected from fresh mouse blood and washed with PBS twice. Then, the red blood cells were co-incubated with different concentrations of PMOF@HA at 37 °C. After incubation for 6 h, the mixtures were centrifugated to obtain the red blood cells, and the absorbance at 540 nm of the supernatants was further detected to calculate the hemolysis rates of various groups.

Anti-Tumor Effect in vivo

Balb/c nude mice were obtained from China Wushi, Inc. (Shanghai, China). All animal experiments were approved by the Animal Ethics Committee of Xi'an Jiaotong University [No. XJTUSLS (2023) 77] and were conducted according to the institutional guidelines. SMMC-7721 cells (2×10^6) were injected subcutaneously in the rear right flanks of mice to establish tumor-bearing mice. The tumor-bearing mice were used for animal experiments when the tumor volume was up to about 50–100 mm^3.

The tumor-bearing mice were divided into 5 groups with 5 mice in each group randomly, including PBS group, PBS + laser (L) group, PMOF@HA group, MOF@HA + L group and PMOF@HA + L group. The mice were intratumorally injected with 50 μL of PBS buffer or nanosheets (TCPP: 2 mg/kg). After 12 h, the tumors were irradiated with 670 nm laser (100 mW/cm^2) for 10 min. The tumor volume was monitored and calculated following the below formula:

$$V = \text{length} \times \text{width}^2/2$$

At day 16, the mice were sacrificed and the tumors were excised for hematoxylin and eosin (H&E) staining, Ki67 and HIF-1α immunohistochemical staining.

Statistical Analysis

Prism 6 software (GraphPad) was used for statistical analysis. Data was expressed as mean ± standard deviation (SD). One-way analysis of variance (ANOVA) or *t*-test was used to evaluate the statistical significance. The significance was denoted as $*P < 0.05$, $**P < 0.01$, $***P < 0.001$. A *P*-value <0.05 was considered as statistically significant.

Results and Discussion

Preparation and Characterization of PMOF@HA

The MOF nanosheets were synthesized via the solvothermal reaction with TCPP utilizing the organic ligands and Zr^{4+} as the metal nodes. As shown in Figure 1A, the MOF nanosheets exhibited a typical two-dimensional lamellar structure. After in situ generation of Pt nanoparticles, a multitude of nanoscale black dots (indicated as Pt nanoparticles) were distinctly observable on the surface of PMOF, as demonstrated in the TEM images (Figure 1B). Next, HA was coated onto the outer layer of PMOF via electrostatic interaction, resulting in the final PMOF@HA without any discernible changes in their structures (Figure 1C). The content of Pt element in PMOF@HA was about 8.25 ± 0.81% detected by ICP-MS assay. Besides, the PMOF@HA also demonstrated good stability without any visible signs of aggregation when stored in PBS buffer or PBS buffer containing 10% FBS for a duration of 4 days (Figure S1). The zeta potentials of different formulations were determined using a Zetasizer Nano-ZS system. As shown in Figure 1D, the zeta potential of MOF nanosheets was 41.5 mV, ascribing to the incomplete coordination of Zr^{4+} on the surface of nanosheets. Upon the introduction of Pt nanoparticles, the zeta potential of PMOF decreased to 26.1 mV. Thus, PMOF could further adsorb negatively charged HA, resulting in a shift of the zeta potential from positive to negative (−17.4 mV). FT-IR spectra were also conducted to characterize the PMOF@HA nanosheets. As shown in Figure S2, the absorption peaks at 655 cm^{-1} in all nanosheets were assigned to Zr-O bonds and Pt nanoparticles modification caused a sharp absorption peak appeared at 1050 cm^{-1} in PMOF nanosheets.[37,38] Besides, an intensified absorption peak at 1614 cm^{-1}, corresponding to the asymmetric stretching vibration of carboxylate anion,[39] was found in PMOF@HA compared with PMOF, indicating the successful HA coating again. The XRD patterns were depicted in Figure S3, MOF had the similar peaks to the Zr-TCPP nanosheets reported in the previous literature,[40] and the further modification of Pt nanoparticles had little influence on its characteristic peaks. The TEM mapping assay also provided powerful

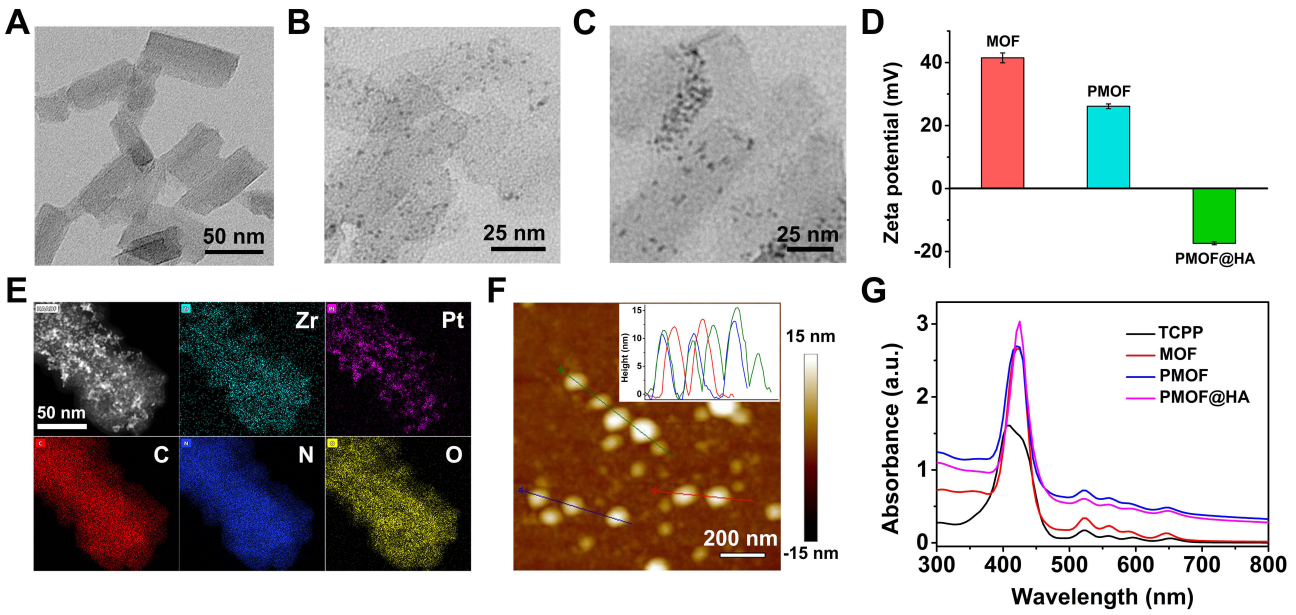

Figure 1 TEM images of (**A**) MOF, (**B**) PMOF and (**C**) PMOF@HA. (**D**) Zeta potentials of different formulations. (**E**) TEM mapping of PMOF@HA. (**F**) AFM image of MOF nanosheets (inset is the height profile corresponding to the line with different colors in the AFM image). (**G**) UV-Vis spectra of TCPP, MOF, PMOF and PMOF@HA.

evidence for the presence of Pt nanoparticles decoration on the PMOF@HA (Figure 1E). The thickness of MOF nanosheets was determined to be about 11.65 nm via AFM (Figure 1F). The characteristic peaks of UV-Vis spectra at 415, 516, 550, 595 and 645 nm, attributed to the B- and Q-band absorption of TCPP, were observed in all the spectra of each intermediate and the final PMOF@HA, indicating that the formation of MOF nanosheet had no influence on the absorption of organic ligand TCPP (Figure 1G).

$^1O_2$ Generation Capacity of PMOF@HA

The $^1O_2$ generation capability of PMOF@HA was investigated using a SOSG detection probe, where the fluorescence intensity of SOSG correlated positively with $^1O_2$ level in the solution. As shown in Figure 2A and S4, the fluorescence intensity of SOSG in the solution containing MOF, PMOF and PMOF@HA all had a prominent increase after 670 nm laser irradiation. By comparison, the fluorescence spectra of SOSG in the groups containing nanosheets without laser irradiation or that only with laser irradiation showed no significant changes. The above results demonstrated that the PMOF@HA possessed excellent $^1O_2$ production ability, and the modification of Pt nanoparticles and HA hardly changed its PDT property. Besides, as shown in Figure 2B and C, with the increase of irradiation time, the SOSG fluorescence intensity in the solution with PMOF@HA increased rapidly, while the SOSG fluorescence intensity in Control group still maintained at a low level. And the relative fluorescence intensity (F_t/F_0) of SOSG probe in the solution containing PMOF@HA exhibited an approximately four-fold enhancement after 15 min of irradiation. Notably, this enhancement demonstrated a nearly linear dependence on the duration of irradiation, indicating the outstanding photostability of PMOF@HA under light exposure for continuous $^1O_2$ production (Figure 2D), unlike common PSs often suffering from photobleaching issues.

Additionally, Pt nanoparticles, as a kind of nanozymes, showed catalase-like activity for catalyzing the decomposition of H_2O_2 into O_2. Thus, we next evaluated the O_2 generation capability of Pt nanoparticles-decorated PMOF@HA. As shown in Figure 2E, the solution containing both PMOF@HA and H_2O_2 exhibited a huge O_2 increase of around 15 mg/mL, which indicated that the decoration of Pt nanoparticles could endow PMOF@HA with catalase-like activity. Furthermore, under 670 nm laser irradiation, the PMOF@HA + H_2O_2 group had the highest $^1O_2$ production, with the fluorescence intensity of SOSG being about 1.5 times stronger than that of PMOF@HA and MOF@HA + H_2O_2 groups, suggesting that the self-supply of O_2 could intensify the $^1O_2$ generation of PMOF@HA (Figure 2F).

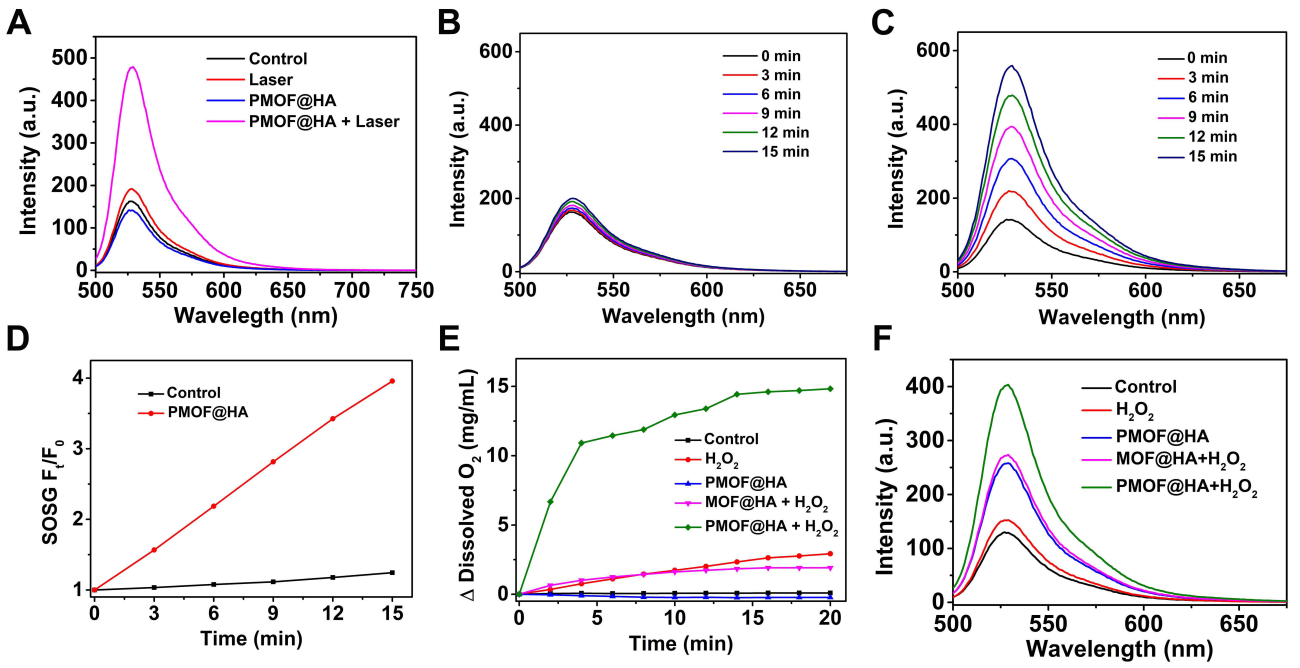

Figure 2 (**A**) Fluorescence spectra of SOSG in the absence or presence of PMOF@HA with or without laser irradiation. Fluorescence spectra of SOSG in the (**B**) absence or (**C**) presence of PMOF@HA with laser irradiation for different times. (**D**) The time-dependence of relative fluorescence intensity of SOSG at 540 nm. (**E**) Dissolved O_2 concentrations of different groups. (**F**) Fluorescence spectra of SOSG in the solution containing different components.

Cell Uptake

CD44 is overexpressed in many cancer types, thereby nanoparticles modified with its ligand HA could significantly enhance the capability of targeted delivery.[41] Firstly, we assessed the CD44 expression level on SMMC-7721 and 293T cells via flow cytometry. As shown in Figure 3A and B, SMMC-7721 cells had an extraordinarily high CD44 expression, while the 293T cells displayed a significantly lower expression. Thus, the fluorescence intensity inside SMMC-7721 cell was more than 2 times higher than that inside 293T cells, irrespective of the 4 h or 8 h co-incubated with Cy5 labelled PMOF@HA, indicating the enhanced uptake of PMOF@HA by SMMC-7721 cells (Figure 3C, D and S5). However,

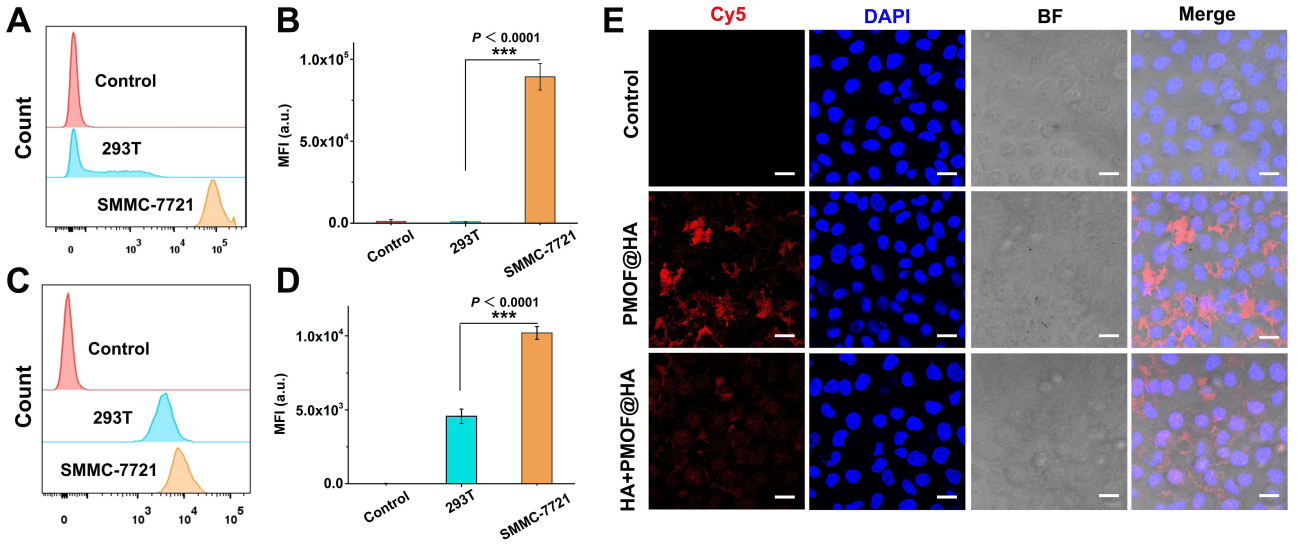

Figure 3 (**A**) Flow cytometry analysis of CD44 expression in SMMC-7721 and 293T cells. (**B**) The corresponding mean fluorescence intensity (MFI) in (**A**) (n = 3). (**C**) Flow cytometry analysis of Cy5 fluorescence inside cells after incubated with Cy5-labeled PMOF@HA for 8 h. (**D**) The corresponding mean fluorescence intensity (MFI) in (**C**) (n = 3). (**E**) CLSM images of SMMC-7721 cells incubated with Cy5-labeled PMOF@HA. ***$P < 0.001$.

a significant decrease of Cy5 (red) fluorescence was found in the cells pre-treated with excess HA to block CD44 (Figure 3E), further elucidating the enhanced cell internalization induced by CD44 receptor.

Next, we investigated the cytotoxicity of PMOF@HA to SMMC-7721 and 293T cells. Notably, PMOF@HA showed little toxicity to both the cell types in the absence of external laser irradiation, with the cell viabilities remaining above 90% even at TCPP concentration of up to 240 μg/mL (Figure 4A). These results unequivocally demonstrated the low dark toxicity of our prepared PMOF@HA nanosheets.

Hypoxia Relief and ROS Production in vitro

To confirm hypoxia relief function of Pt-nanozyme decorated PMOF@HA within cancer cells, an oxygen detection probe $[Ru(dpp)_3]Cl_2$, was employed to explore the hypoxic situation inside cells, as its fluorescence intensity was noted to be negatively correlated with the intracellular O_2 level. As shown in Figure 4B, all groups exhibited negligible red fluorescence when the cells cultured under normoxic situation. However, under hypoxia, the red fluorescence intensities in the untreated cells or cells treated with MOF@HA increased significantly, highlighting severe hypoxia inside cells. In contrast, the cells co-incubated with PMOF@HA showed only a slight increase in red fluorescence when the culture conditions were changed to hypoxia, verifying that PMOF@HA with catalase-like activity could relieve intracellular

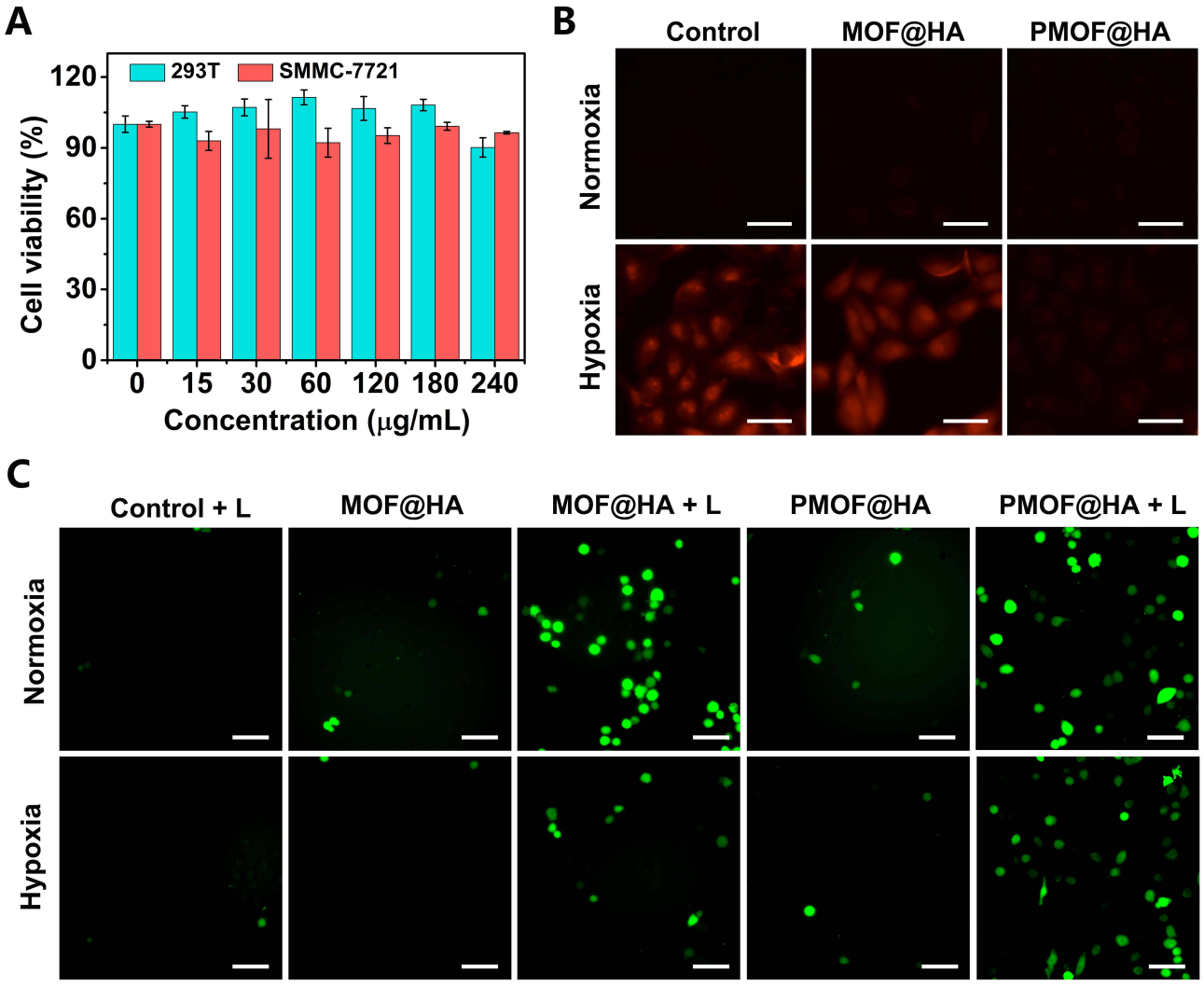

Figure 4 (**A**) Cell viabilities of 293T and SMMC-7721 cells incubated with PMOF@HA nanosheets for 48 h (n = 4). (**B**) Fluorescence microscope images of the O_2 detection probe $[Ru(dpp)_3]Cl_2$ inside the cells with different treatments. Scale bar = 20 μm. (**C**) Fluorescence microscope images of intracellular ROS detection probe DCFH-DA inside cells with different treatments. Scale bar = 50 μm.

hypoxic condition effectively. Benefitting from the O_2 generation ability, PMOF@HA could further stimulate the production of large amounts of ROS and augment intracellular oxidative stress level under hypoxic condition after 670 nm laser irradiation, as indicated by the intense green fluorescence emitted from ROS detection probes inside cells (Figure 4C). These results highlighted the excellent ROS production ability of PMOF@HA nanosheets in hypoxic cells, relying on its O_2 self-supply induced by catalase-like activity.

PDT of PMOF@HA in vitro

Subsequently, we evaluated the PDT killing effect of PMOF@HA on SMMC-7721 cells. As shown in Figure 5A, both MOF@HA and PMOF@HA exerted good killing effect on cancer cells cultured under normoxic condition, with cell viabilities reducing by more than 70% at a TCPP concentration of 120 μg/mL. However, the PDT effect of MOF@HA was severely compromised under hypoxic conditions, with the cell killing efficiency induced by MOF@HA (TCPP: 120 μg/mL) and laser irradiation reaching only about 40% (Figure 5B). Intriguingly, PMOF@HA still displayed an outstanding killing effect, with the cell viability declining to below 20% at the TCPP concentration of 120 μg/mL, even under hypoxic conditions. Additionally, the cell viabilities of normal 293T cells treated with PMOF@HA and laser were also assessed (Figure S6). The lower PDT killing effect to 293T cells compared with SMMC-7721 cells indicated the targeted PDT ability of PMOF@HA, ascribing to the enhanced cell uptake of cancer cells to PMOF@HA illustrated in Figure 3.

Meanwhile, the live/death cell staining was conducted to further assess the cell killing effect of PMOF@HA intuitively. As shown in Figure 5C, upon 670 nm laser irradiation, the PDT killing effect of both MOF@HA and PMOF@HA was consistent with the CCK-8 assay. While amounts of cells were observed to be still alive when treated with MOF@HA and laser irradiation under hypoxia, only little green fluorescence (representing living cells) appeared inside the cells treated with PMOF@HA and laser irradiation under both normoxic and hypoxic conditions. Additionally, cell apoptosis caused by the PDT of PMOF@HA was also detected using flow cytometry (Figure 5D). Among all the groups, the PMOF@HA + L group showed the highest cell apoptosis rate of 89.98% under normoxia and 79.77% under

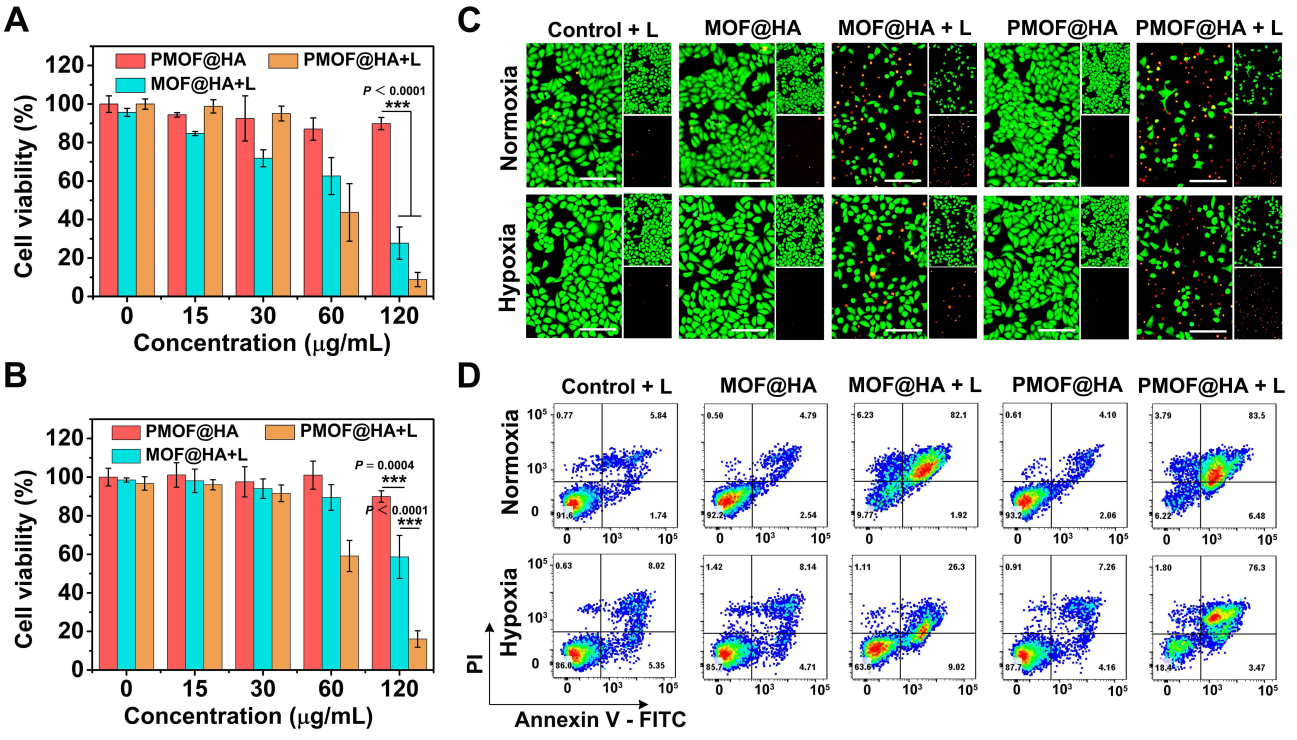

Figure 5 Cell viabilities of SMMC-7721 cells with different treatments under (**A**) normoxic and (**B**) hypoxic conditions (n = 4). (**C**) Fluorescence microscope images of SMMC-7721 cells stained with Calcein AM and PI. Scale bar = 100 μm. (**D**) Flow cytometry analysis of the apoptosis of SMMC-7721 cells with different treatments under normoxic and hypoxic conditions. ***$P < 0.001$.

hypoxia. Therefore, all the above results underscored that PMOF@HA, with its capacity of O_2 self-supply, could significantly reinforce the PDT effect against cancer cells under hypoxic conditions.

Anti-Tumor Effect of PMOF@HA in vivo

The hemolysis assay was first conducted to demonstrate the good blood compatibility of PMOF@HA with a low hemolysis rate under the experimental concentration (Figure S7). Then, we further constructed a tumor model in nude mice and investigated the tumor inhibition capability of PMOF@HA in vivo. The intratumorally injected PMOF@HA exhibited a good enrichment and retention at tumor sites (Figure S8), which was helpful to enhance the killing effects of PDT and simultaneously lowered the toxic risks to main organs. The anti-tumor effects are depicted in Figure 6A, the tumors in PBS, PBS + L and PMOF@HA groups all grew rapidly, signifying the negligible tumor suppression attributed to laser irradiation or PMOF@HA alone. With 670 nm laser irradiation, MOF@HA showed moderate tumor inhibition due to the limited PDT effect on hypoxic solid tumor. Remarkably, the mice treated with PMOF@HA and laser irradiation exhibited the strongest anti-tumor efficacy, ascribing to the hypoxia relief ability of PMOF@HA during PDT treatment. The tumor suppression effect of PMOF@HA with laser irradiation was further reflected by the smallest tumor volume and the lightest average tumor mass (Figure 6B and C).

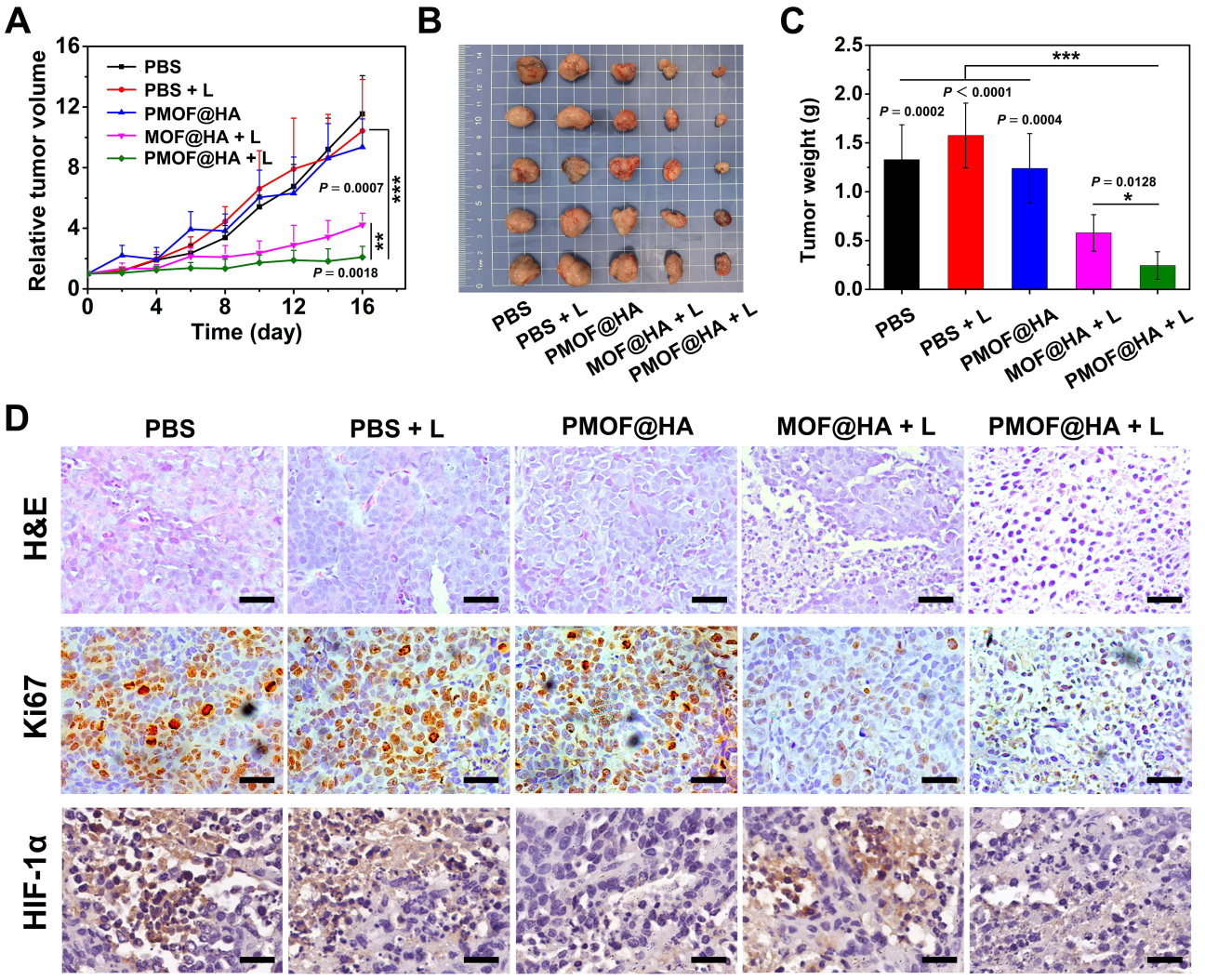

Figure 6 (**A**) Tumor growth curves, (**B**) ex vivo tumor photographs and (**C**) average tumor weights of mice in different groups (n = 5). (**D**) Optical microscope images of tumor H&E staining, Ki67 and HIF-1α immunohistochemical staining. Scale bar = 20 μm. *P < 0.05, **P < 0.01, ***P < 0.001.

In addition, the excised tumor tissues at the end of treatment were sectioned for H&E pathological staining, Ki67 and HIF-1α immunohistochemical staining. As shown in Figure 6D, the tumor treated with PMOF@HA and laser irradiation displayed severe cell morphology destruction and nucleus shrinkage, along with significantly reduced proliferation indicated by a decrease in Ki67-positive cells. Importantly, the tumor tissues treated with PMOF@HA exhibited a notable decrease in HIF-1α levels compared with other groups, providing strong evidences that PMOF@HA could alleviate the hypoxic microenvironment within solid tumor, thereby reinforcing the subsequent PDT killing effect of itself. Throughout the treatment period, there were no significant changes in average body weight of each group (Figure S9), suggesting the low systemic toxicity of our therapeutic paradigms. Overall, all the above results verified that the Pt-nanozyme decorated PMOF@HA, with their HA-targeted uptake and catalase-like activity for O_2 self-supply, represents a promising anti-tumor agent to enhance PDT efficacy against hypoxic tumor.

Conclusion

In summary, we successfully developed Pt nanozyme-decorated porphyrin MOF nanosheets. PMOF@HA could realize targeted uptake by CD44 overexpressed tumor cells, facilitated by the HA coating. Most importantly, the unique 2D structure of PMOF@HA tremendously improved the photochemical property of porphyrin PS, such as avoiding aggregation, increasing photo-sensitivity to external light and facilitating rapid diffusion of generated ROS. Simultaneously, this structure provided an excellent platform for the ornamentation of Pt nanozymes and the display of their catalase-like activities to catalyze H_2O_2 in situ for O_2 production. In vitro and in vivo experiments demonstrated that PMOF@HA could be internalized more effectively by cancer cells, generating abundant $^1O_2$ through O_2 self-supply to eliminate cancer cells and suppress tumor growth. The combination of 2D MOF nano-PSs and Pt nanozymes provides a simple but effective strategy to surmount the dilemma of poor PDT efficacy against hypoxic tumors. However, the laser penetration depth is another key factor that significantly affects the PDT effect against solid tumor in deep tissue. Many efforts have been made to bypass the limitations of insufficient penetration depth of laser, such as PDT based on up-conversion nanoparticles (UCNPs) or scintillating nanoparticles, development of novel PSs with longer excitation wavelengths and so on. In the future work, an excellent PDT system that simultaneously overcomes tumor hypoxia and low laser penetration depth deserves to be further pursued for us.

Acknowledgments

This work was supported by the National Natural Science Foundation of China (62175198, U22A2092 and 62275212), the Fundamental Research Funds for the Central Universities (xtr062022002), and the Key Research and Development Projects of Shaanxi Province (2022ZDLSF04-09).

Disclosure

The authors report no conflicts of interest in this work.

References

1. Lan M, Zhao S, Liu W, Lee CS, Zhang W, Wang P. Photosensitizers for photodynamic therapy. *Adv Healthc Mater*. 2019;8(13):e1900132. doi:10.1002/adhm.201900132
2. Juarranz A, Jaen P, Sanz-Rodriguez F, Cuevas J, Gonzalez S. Photodynamic therapy of cancer. Basic principles and applications. *Clin Transl Oncol*. 2008;10(3):148–154. doi:10.1007/s12094-008-0172-2
3. Zhang Q, He J, Yu W, et al. A promising anticancer drug: A photosensitizer based on the porphyrin skeleton. *RSC Med Chem*. 2020;11(4):427–437. doi:10.1039/c9md00558g
4. Hamblin MR. Photodynamic therapy for cancer: What's past is prologue. *Photochem Photobiol*. 2020;96(3):506–516. doi:10.1111/php.13190
5. Yano S, Hirohara S, Obata M, et al. Current states and future views in photodynamic therapy. *J Photochem Photobiol C*. 2011;12(1):46–67. doi:10.1016/j.jphotochemrev.2011.06.001
6. Ni N, Zhang X, Ma Y, et al. Biodegradable two-dimensional nanomaterials for cancer theranostics. *Coord Chem Rev*. 2022;458:214415. doi:10.1016/j.ccr.2022.214415
7. Liu C, Qin H, Kang L, et al. Graphitic carbon nitride nanosheets as a multifunctional nanoplatform for photochemical internalization-enhanced photodynamic therapy. *J Mater Chem B*. 2018;6(47):7908–7915. doi:10.1039/c8tb02535e
8. Qin L, Jiang S, He H, Ling G, Zhang P. Functional black phosphorus nanosheets for cancer therapy. *J Control Release*. 2020;318:50–66. doi:10.1016/j.jconrel.2019.12.013
9. Zhu J, Ouyang N, Zhao R, et al. Black phosphorus nanosheets grafted with gold nanorods and carbon nanodots for synergistic antitumor therapy. *ACS Appl Mater Interfaces*. 2023;15(22):26241–26251. doi:10.1021/acsami.3c00524

10. Xie M, Gao R, Li K, et al. O_2-generating fluorescent carbon dot-decorated MnO_2 nanosheets for "Off/On" MR/fluorescence imaging and enhanced photodynamic therapy. *ACS Appl Mater Interfaces*. 2023;15(49):56717–56732. doi:10.1021/acsami.3c12155
11. Zeng D, Wang L, Tian L, Zhao S, Zhang X, Li H. Synergistic photothermal/photodynamic suppression of prostatic carcinoma by targeted biodegradable MnO_2 nanosheets. *Drug Deliv*. 2019;26(1):661–672. doi:10.1080/10717544.2019.1631409
12. Alves SR, Calori IR, Tedesco AC. Photosensitizer-based metal-organic frameworks for highly effective photodynamic therapy. *Mater Sci Eng C*. 2021;131:112514. doi:10.1016/j.msec.2021.112514
13. Lan G, Ni K, Lin W. Nanoscale metal-organic frameworks for phototherapy of cancer. *Coord Chem Rev*. 2019;379:65–81. doi:10.1016/j.ccr.2017.09.007
14. Zhang L, Ng G, Kapoor-Kaushik N, et al. 2D porphyrinic metal–organic framework nanosheets as multidimensional photocatalysts for functional materials. *Angew Chem Int Ed*. 2021;60(42):22664–22671. doi:10.1002/anie.202107457
15. Li B, Wang X, Chen L, et al. Ultrathin Cu-TCPP MOF nanosheets: A new theragnostic nanoplatform with magnetic resonance/near-infrared thermal imaging for synergistic phototherapy of cancers. *Theranostics*. 2018;8(15):4086–4096. doi:10.7150/thno.25433
16. Mu J, He L, Fan W, et al. Cascade reactions catalyzed by planar metal-organic framework hybrid architecture for combined cancer therapy. *Small*. 2020;16(42):e2004016. doi:10.1002/smll.202004016
17. Lismont M, Dreesen L, Wuttke S. Metal-organic framework nanoparticles in photodynamic therapy: Current status and perspectives. *Adv Funct Mater*. 2017;27(14):1606314. doi:10.1002/adfm.201606314
18. Xu D, Duan Q, Yu H, Dong W. Photodynamic therapy based on porphyrin-based metal-organic frameworks. *J Mater Chem B*. 2023;11(26):5976–5989. doi:10.1039/d2tb02789e
19. Zhu W, Yang Y, Jin Q, et al. Two-dimensional metal-organic-framework as a unique theranostic nano-platform for nuclear imaging and chemo-photodynamic cancer therapy. *Nano Res*. 2019;12(6):1307–1312. doi:10.1007/s12274-018-2242-2
20. Dai X, Huo M, Zhang B, Liu Z, Liu Y. Folic acid-modified cyclodextrin multivalent supramolecular assembly for photodynamic therapy. *Biomacromolecules*. 2022;23(9):3549–3559. doi:10.1021/acs.biomac.2c00276
21. Meng HM, Hu XX, Kong GZ, et al. Aptamer-functionalized nanoscale metal-organic frameworks for targeted photodynamic therapy. *Theranostics*. 2018;8(16):4332–4344. doi:10.7150/thno.26768
22. Feng L, Chen M, Li R, et al. Biodegradable oxygen-producing manganese-chelated metal organic frameworks for tumor-targeted synergistic chemo/photothermal/photodynamic therapy. *Acta Biomater*. 2022;138:463–477. doi:10.1016/j.actbio.2021.10.032
23. Zhang C, Qin W-J, Bai X-F, Zhang X-Z. Nanomaterials to relieve tumor hypoxia for enhanced photodynamic therapy. *Nano Today*. 2020;35:100960. doi:10.1016/j.nantod.2020.100960
24. Liu X, Jansman MMT, Hosta-Rigau L. Haemoglobin-loaded metal organic framework-based nanoparticles camouflaged with a red blood cell membrane as potential oxygen delivery systems. *Biomater Sci*. 2020;8(21):5859–5873. doi:10.1039/d0bm01118e
25. Day RA, Sletten EM. Perfluorocarbon nanomaterials for photodynamic therapy. *Curr Opin Colloid Interface Sci*. 2021;54:101454. doi:10.1016/j.cocis.2021.101454
26. Cheng Y, Cheng H, Jiang C, et al. Perfluorocarbon nanoparticles enhance reactive oxygen levels and tumour growth inhibition in photodynamic therapy. *Nat Commun*. 2015;6:8785. doi:10.1038/ncomms9785
27. Wan Y, Fu LH, Li C, Lin J, Huang P. Conquering the hypoxia limitation for photodynamic therapy. *Adv Mater*. 2021;33(48):e2103978. doi:10.1002/adma.202103978
28. Phua SZF, Yang G, Lim WQ, et al. Catalase-integrated hyaluronic acid as nanocarriers for enhanced photodynamic therapy in solid tumor. *ACS Nano*. 2019;13(4):4742–4751. doi:10.1021/acsnano.9b01087
29. Yang X, Liu R, Zhong Z, et al. Platinum nanoenzyme functionalized black phosphorus nanosheets for photothermal and enhanced-photodynamic therapy. *Chem Eng J*. 2021;409:127381. doi:10.1016/j.cej.2020.127381
30. Lin T, Zhao X, Zhao S, et al. O_2-generating MnO_2 nanoparticles for enhanced photodynamic therapy of bladder cancer by ameliorating hypoxia. *Theranostics*. 2018;8(4):990–1004. doi:10.7150/thno.22465
31. Hao Y, Chen Y, He X, et al. RGD peptide modified platinum nanozyme co-loaded glutathione-responsive prodrug nanoparticles for enhanced chemo-photodynamic bladder cancer therapy. *Biomaterials*. 2023;293:121975. doi:10.1016/j.biomaterials.2022.121975
32. Gong L, Zhang Y, Zhao J, et al. All-in-one biomimetic nanoplatform based on hollow polydopamine nanoparticles for synergistically enhanced radiotherapy of colon cancer. *Small*. 2022;18(14):e2107656. doi:10.1002/smll.202107656
33. Shi P, Sun X, Yuan H, Chen K, Bi S, Zhang S. Nanoscale metal-organic frameworks combined with metal nanoparticles and metal oxide/peroxide to relieve tumor hypoxia for enhanced photodynamic therapy. *ACS Biomater Sci Eng*. 2023;9(10):5441–5456. doi:10.1021/acsbiomaterials.3c00509
34. Bao Y, Chen J, Qiu H, et al. Erythrocyte membrane-camouflaged PCN-224 nanocarriers integrated with platinum nanoparticles and glucose oxidase for enhanced tumor sonodynamic therapy and synergistic starvation therapy. *ACS Appl Mater Interfaces*. 2021;13(21):24532–24542. doi:10.1021/acsami.1c05644
35. Chen J, Bao Y, Song Y, et al. Hypoxia-alleviated nanoplatform to enhance chemosensitivity and sonodynamic effect in pancreatic cancer. *Cancer Lett*. 2021;520:100–108. doi:10.1016/j.canlet.2021.07.008
36. Zhu L, Gui T, Song P, et al. Metal-organic framework PCN-224 integrated with manganese dioxide, platinum nanoparticles, and glucose oxidase for enhanced cancer chemodynamic therapy. *ACS Appl Nano Mater*. 2023;6(9):7446–7455. doi:10.1021/acsanm.3c00610
37. Tong H, He R, Chen G, et al. Synthesis of a novel cost-effective double-ligand Zr-based MOF via an inverted modulator strategy towards enhanced adsorption and photodegradation of tetracycline. *J Colloid Interface Sci*. 2024;671:732–741. doi:10.1016/j.jcis.2024.05.211
38. Sun S, Wei C, Xiao Y, Li G, Zhang J. Zirconium-based metal-organic framework gels for selective luminescence sensing. *RSC Adv*. 2020;10(73):44912–44919. doi:10.1039/d0ra09035b
39. Gu D, Liu Y, Li X, et al. Porphyrin-based metal-organic frameworks loaded with Ag nanoparticles and their nanofibrous filters for the photocatalytic reduction of Cr(VI). *Appl Surf Sci*. 2023;614(30):156192. doi:10.1016/j.apsusc.2022.156192
40. Wang H, Ren Y, Feng X, Jiang H. Ultrathin 2D porphyrin-based Zr-MOF nanosheets as heterogeneous catalysts for styrene epoxidation and benzylic C-H oxidation. *ChemCatChem*. 2024;2024:e202400119. doi:10.1002/cctc.202400119
41. Pramanik A, Xu Z, Ingram N, et al. Hyaluronic-acid-tagged cubosomes deliver cytotoxics specifically to CD44-positive cancer cells. *Mol Pharm*. 2022;19(12):4601–4611. doi:10.1021/acs.molpharmaceut.2c00439